

1 **Supplementary Information for “Structure and composition of early**
2 **biofilms formed on dental implants are complex, diverse, subject-**
3 **specific and dynamic”**

4 Short title: Biofilms on implants: supplementary information

5 Sophie Dieckow^{1,*}, Szymon P. Szafranski^{1,2,3,*}, Jasmin Grischke¹, Taoran Qu^{1,2}, Katharina Doll-Nikutta^{1,2},
6 Matthias Steglich^{1,2}, Ines Yang^{1,2}, Susanne Häussler^{3,4,5,6}, and Meike Stiesch^{1,2,3,\$}

7 ¹Department of Prosthetic Dentistry and Biomedical Materials Science, Hannover Medical School,
8 Hannover, Germany

9 ²Lower Saxony Centre for Biomedical Engineering, Implant Research and Development (NIFE),
10 Hannover, Germany

11 ³Cluster of Excellence RESIST (EXC 2155), Hannover Medical School, Hannover, Germany

12 ⁴Department of Molecular Bacteriology, Helmholtz Centre for Infection Research, Braunschweig,
13 Germany

14 ⁵Institute for Molecular Bacteriology, Twincore, Centre for Clinical and Experimental Infection Research,
15 Hannover, Germany.

16 ⁶Department of Clinical Microbiology, Copenhagen University Hospital - Rigshospitalet, Copenhagen,
17 Denmark

18 *Sophie Dieckow and Szymon P. Szafranski contributed equally

19 \$correspondence to: Prof. Dr. Meike Stiesch, Department of Prosthetic Dentistry and Biomedical Materials
20 Science, Hannover Medical School Carl-Neuberg-Str.1 30625 Hannover, Germany; stiesch.meike@mh-
21 hannover.de

22 Table of contents:

23 Supplementary Fig. 1 Confocal images of biofilms formed on implant abutments and biofilm parameters.4

24 Supplementary Fig. 2 Features of biofilm structures 5

25 Supplementary Fig. 3 Composition of biofilms at genus level, their dynamics and their relationships with

26 biofilm parameters..... 6

27 Supplementary Fig. 4 Relationship between bacterial relative abundances at three taxonomic levels..... 7

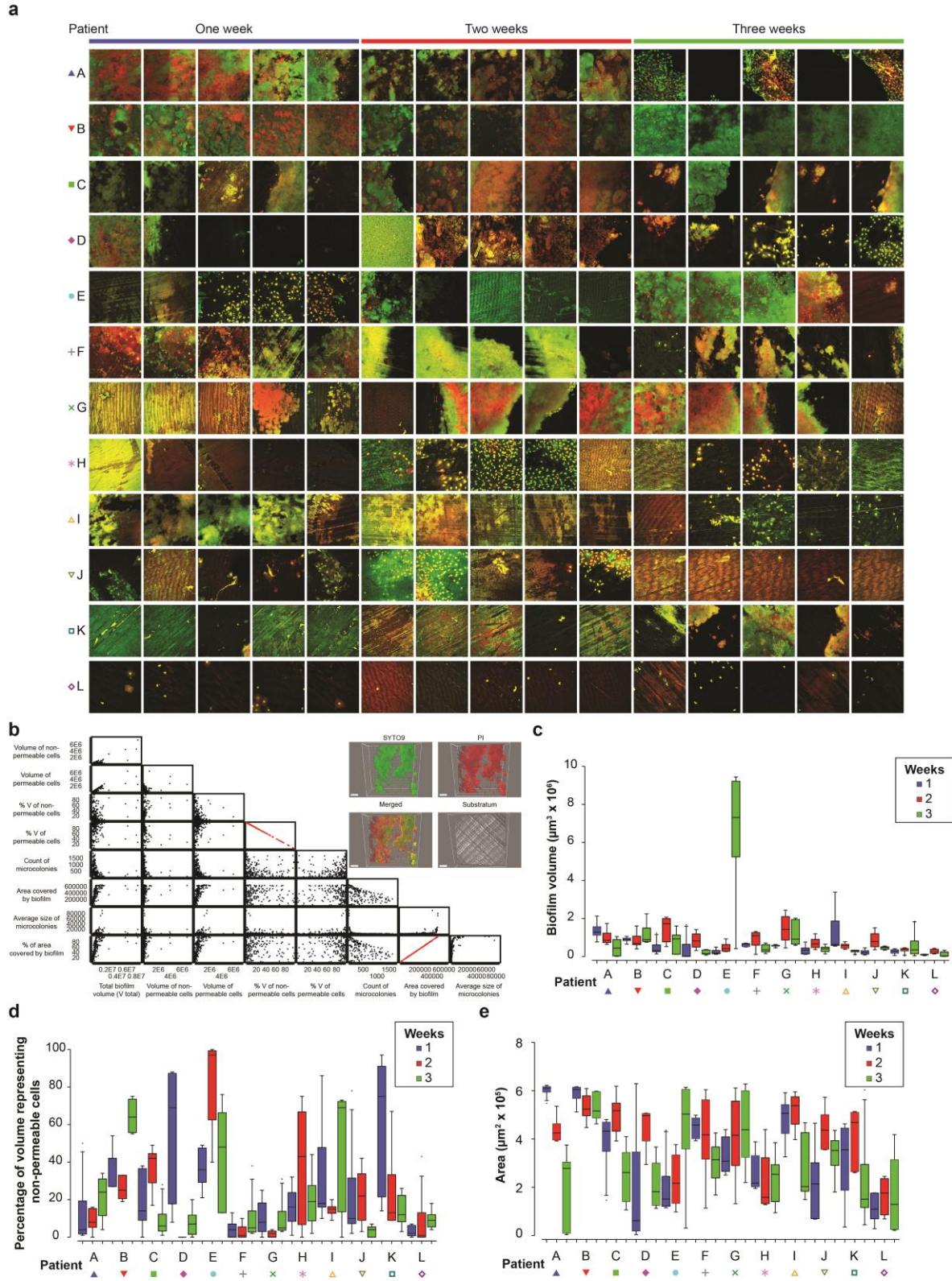
28 Supplementary Fig. 5 Interspecies interaction networks predicted in biofilms..... 9

29 Supplementary Fig. 6 ASV diversity. 11

30 Supplementary File 1. List of microbe-metabolite/enzyme interactions predicted in early biofilms 12

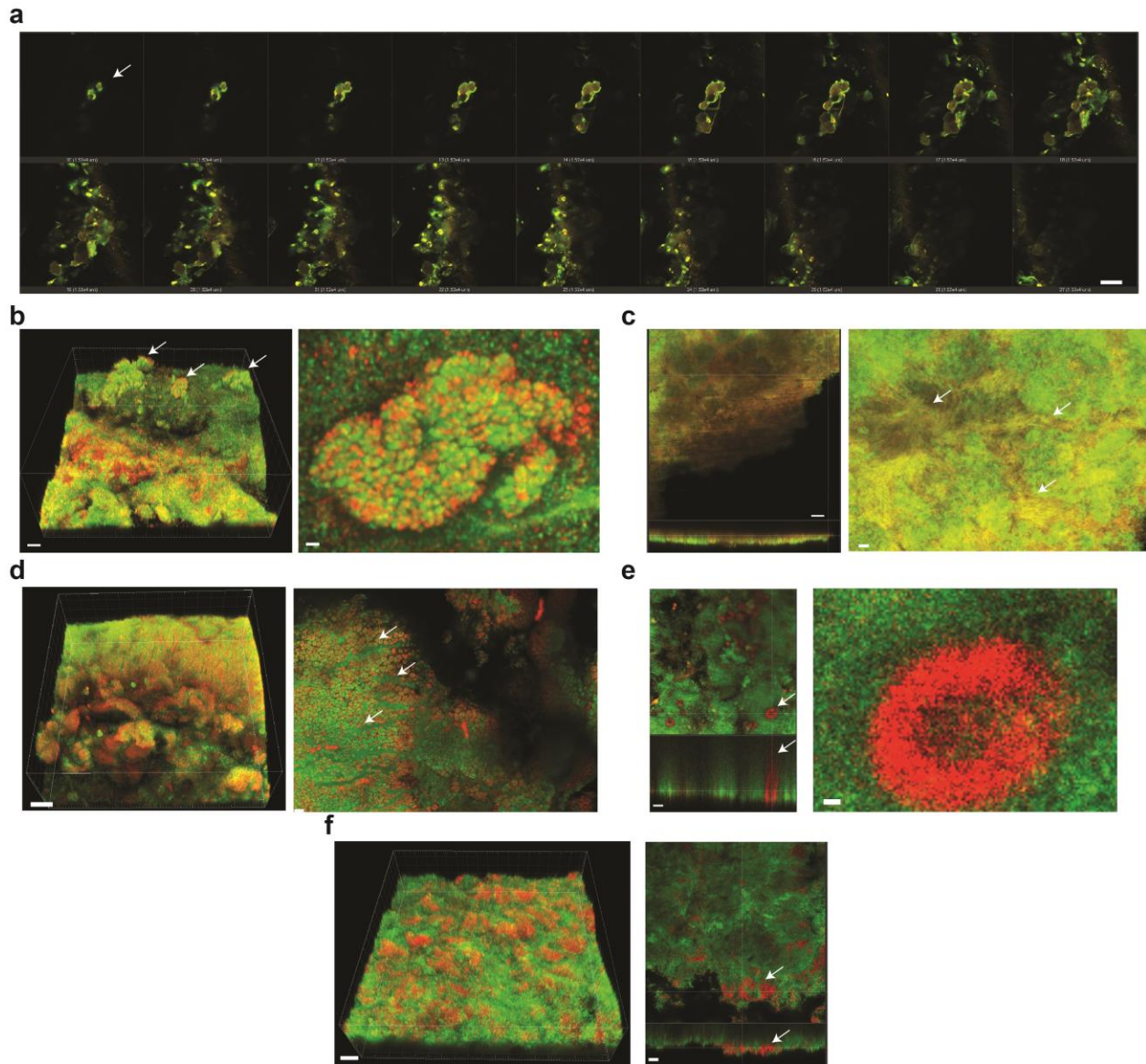
31

32



34 **Supplementary Fig. 1 Confocal images of biofilms formed on implant abutments and biofilm parameters.**

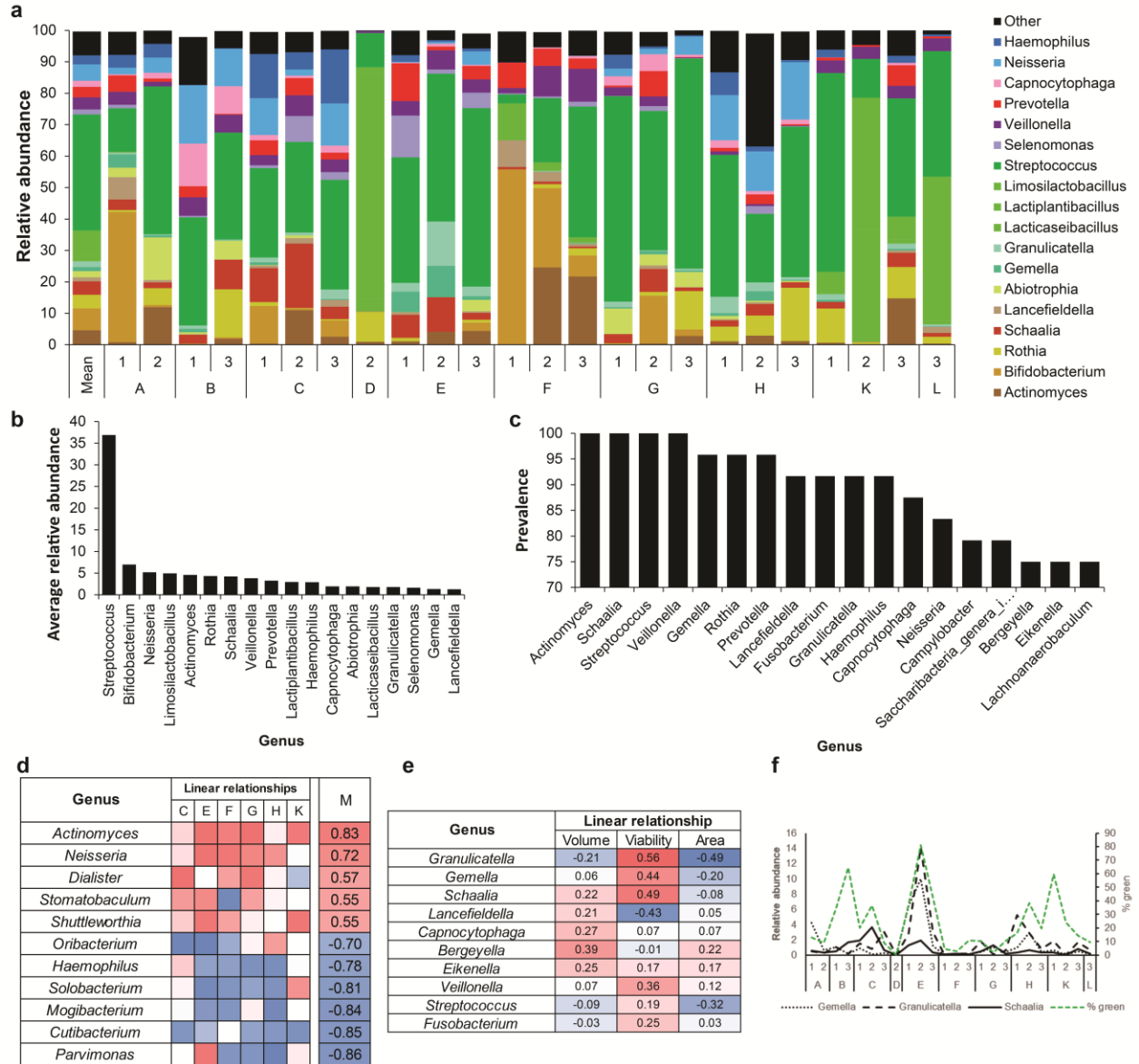
35 **a** CLSM micrographs. Images, which represent maximum intensity projections, are sorted by patients (different rows),
36 age of biofilms in weeks (three sets of columns) and area numbers. Images number 1 to 5, representing all replicates
37 mapped Fig. 1b, are shown from left to right for each week. Each image has a size of 800 μm by 800 μm . In some
38 cases human cells and no or little microbial biofilms were observed. **b** Relationship between biofilm parameters.
39 Scatter plots for pairs of measurements. Highly correlated measurements are indicated in red. Representative
40 micrographs of biofilm shown. The percentage of volume representing non-permeable “live” cells was calculated as
41 the volume of all cells minus the volume of permeable “dead” cells. The bar represents 100 μm . **c – d** Biofilm
42 parameters were calculated as an average value for abutments (five CLSM images each) Box plots ($n = 5$) show all
43 twelve patients indicated by symbols and the three time points indicated by box colors. **c** Biofilm volume. **d** Percent of
44 volume representing non-permeable “live” cells. **e** Area covered by biofilm.



45

46 **Supplementary Fig. 2 Features of biofilm structures**

47 **a** Biofilm from patient J formed by epithelial cells. Biofilm slices are shown. Elevated central surface with steep slope
 48 is indicated with arrow. **b** Biofilm from patient K characterized by aggregates forming vertical projections. Projections
 49 are indicated with arrow in 3D biofilm re-construction (left). Example aggregate was enlarged (right). **c** Biofilm from
 50 patient F characterized by extensive scaffolding. Scaffolding cells were located at the bottom (left). Cell bundles
 51 forming scaffolds were enlarged (right). **d** Biofilm from patient C characterized by aggregates formed by permeable
 52 cells. 3D biofilm re-construction (left). Channels between aggregates filled by distinct population of non-permeable
 53 cells were enlarged (right). **e** Biofilm from patient E characterized by the presence of chimneys. Chimney-like
 54 structures protruded through the entire depth of biofilm (left). Section through chimney-like structure was enlarged
 55 (right). **f** Biofilm from patient B characterized by mosaic of cell clusters. 3D biofilm re-construction (left). Upper
 56 location of aggregates formed by permeable cells is indicated with arrow (right).



57

58 **Supplementary Fig. 3 Composition of biofilms at genus level, their dynamics and their relationships with biofilm parameters**

59

60 **a** Relative abundance of reads grouped at the genus level and plotted for each patient-time point combination as well as for average profile. The most abundant genera are shown, while the reads matching other genera were summed up and plotted together as “Other”.

61

62 **b** Most abundant genera. **c** Most prevalent genera. **d** Pearson’s correlation values between time and abundances of selected genera. Heat map shows correlation values for the abundances of the genera in each patient. Genera are sorted by decreasing median values across patients from top to bottom. Median values are plotted next to the heatmap.

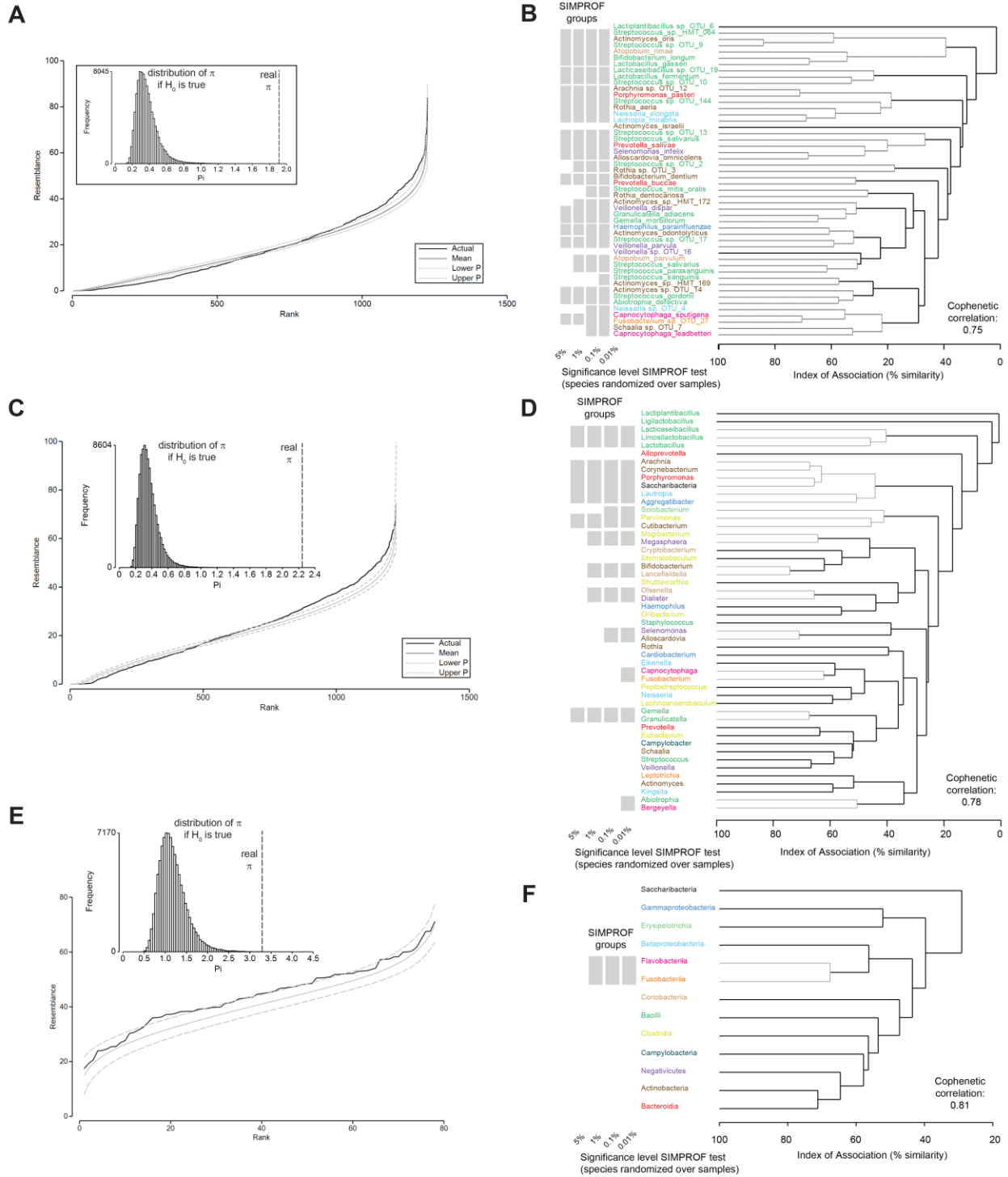
63

64 **e** Correlations between parameters describing biofilm structures and relative abundances for selected genera. Only genera showing absolute values of correlation higher than 0.3 with at least one parameter are shown.

65

66 **f** Coherent variable curves. Line plots of relative abundances (for *Gemella*, *Granulicatella*, and *Schaalia*) and for % of volumes filled by non-permeable cells in biofilm reflecting viability.

67



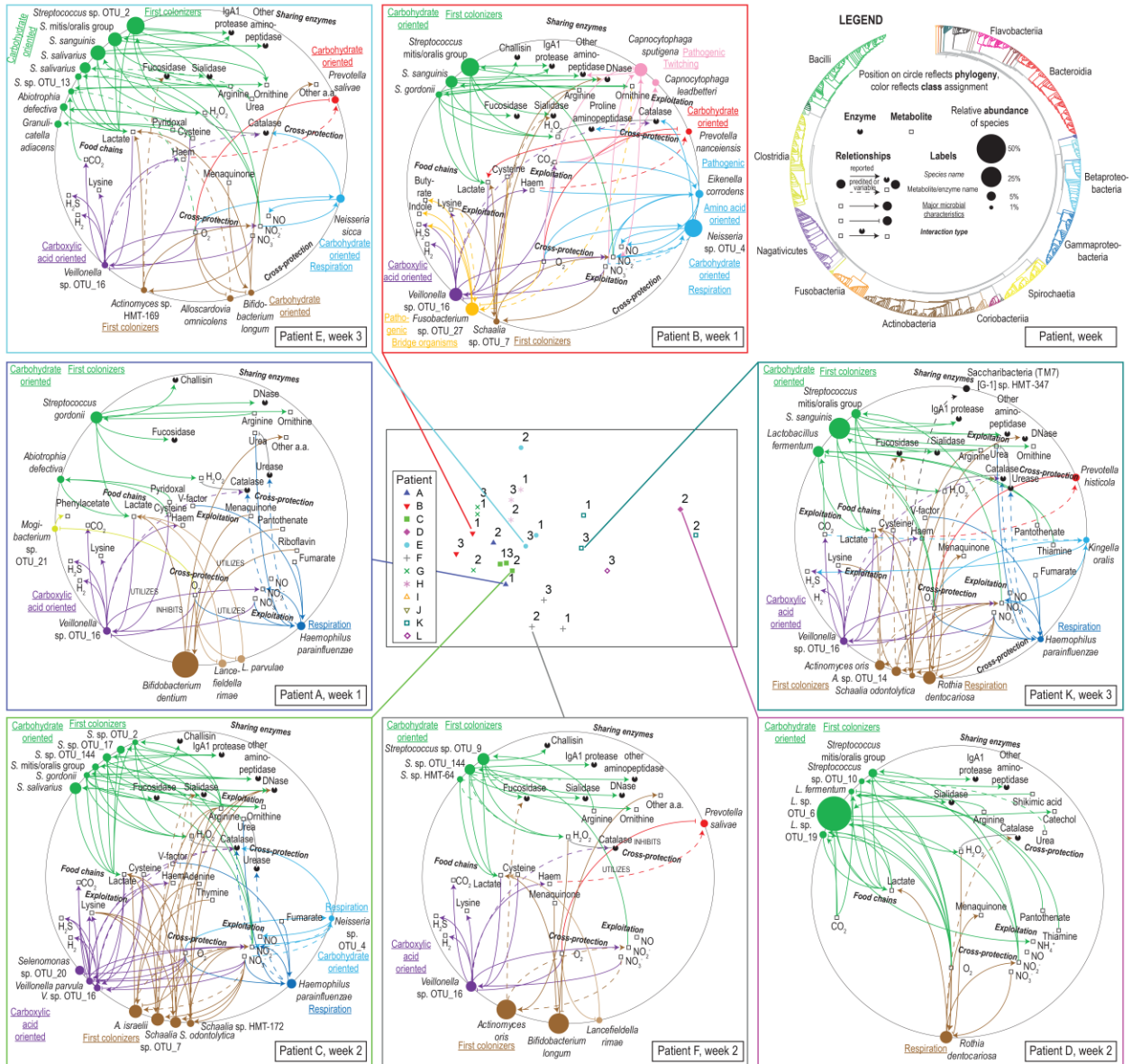
68

69 **Supplementary Fig. 4 Relationship between bacterial relative abundances at three taxonomic levels.**

70 R-mode analysis using pairwise Whittaker's associations was performed for taxa at three different taxonomic levels. **A**
 71 Similarity profile for species. **B** Dendrogram for species. **C** Similarity profile for genera. **D** Dendrogram for genera. **E**
 72 Similarity profile for classes. **F** Dendrogram for classes. Type 2 SIMPROF tests were performed to validate the
 73 hypothesis that there is no associations of any sort among taxa. Values were permuted 100,000 times for each taxon

74 across all samples. Type 3 SIMPROF tests were performed for grouping of taxa detected with type 2 test to validate
75 the hypothesis that the associations within these subsets are not distinguishable, i.e. that the taxa are coherent in their
76 patterns of abundance across the full sample set. This time values orthogonal permutation scheme was applied ($n =$
77 100,000), namely taxa we permuted across the subset of taxa. For each taxonomic levels similarity profile with inset
78 visualizing distribution of the distance π (left), and dendrogram (agglomerative, group average linked) from an index
79 of association matrix among taxa (right) are shown. Similarity profiles were obtained by computing the indices of
80 association, ordering them (y axis) and plotting against their ranks (x axis) to generate continuous black line. Also
81 shown, for each value of x, is the mean index (continuous grey line) from 100,000 permutations of the data matrix
82 (under the null hypothesis), and the range (dashed grey lines) in which 99% of the permuted index values lie. In inset
83 the distribution of the distance π of (a further) 100,000 permuted profiles from the mean profile, in comparison with π
84 for the real profile (seen not to come from the null, establishing the existence of taxon associations). In dendograms
85 grey lines and grey boxes denote the coherent groups of taxa containing more than one taxon. Broad levels of
86 SIMPROF tests (5%, 1%, 0.1%, and 0.01%) were compared to discover stable relationships.

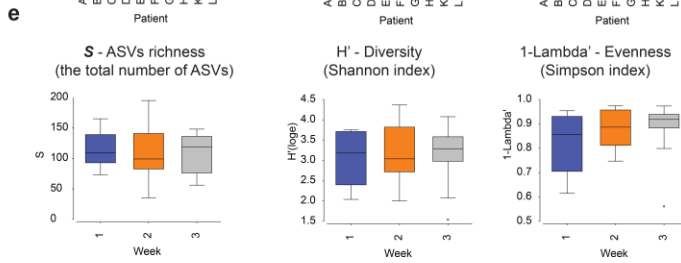
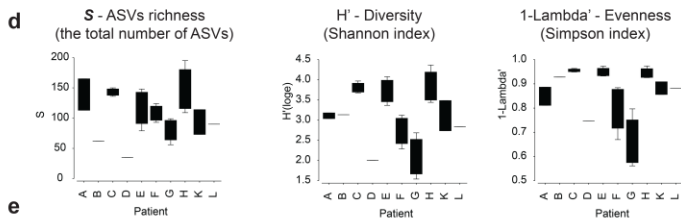
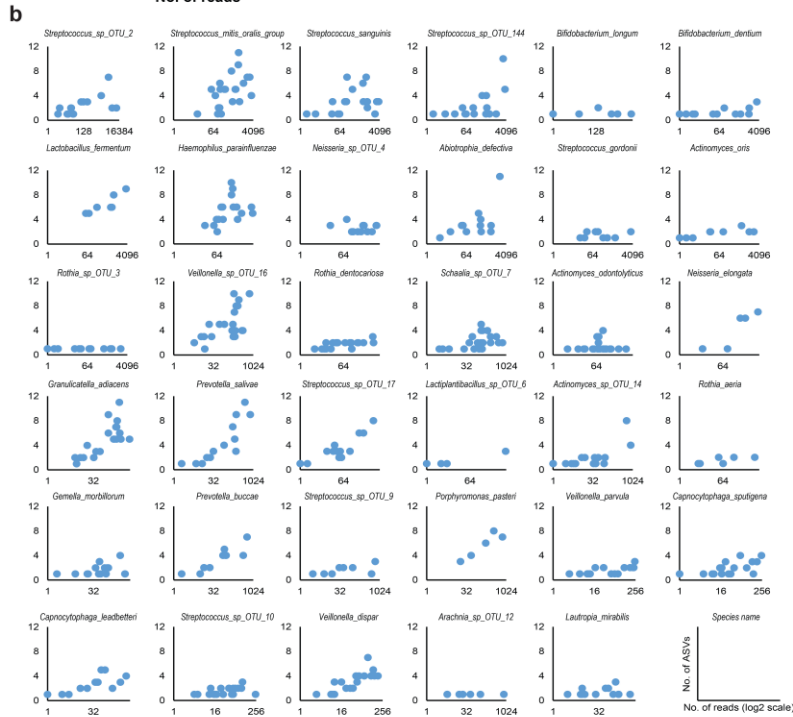
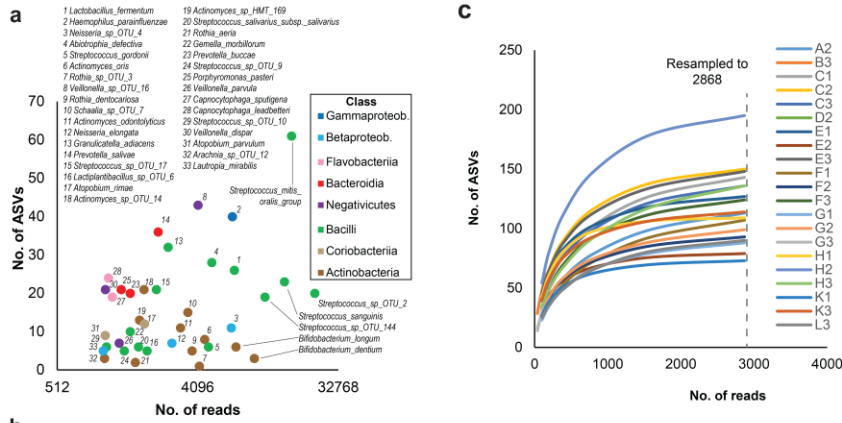
87



88

89 **Supplementary Fig. 5 Interspecies interaction networks predicted in biofilms.**

90 Ecological interactions were inferred using a custom-made database. Briefly, for all taxa that reached at least 2% of
 91 relative abundance, information on interspecies interactions were retrieved from the literature, transformed into a
 92 graph database and visualized using custom-made circular graphs. Ecological profiles are placed in similar orientation
 93 as in Fig. 3, except that the missing ecological profile for patient J was replaced with a comprehensive figure legend.
 94 The ordination in the middle was constructed using the relative abundance of reads grouped to species.



96 **Supplementary Fig. 6 ASV diversity.**

97 **a** ASVs detected for the most abundant species in the studied population, plotted as a function of sequencing depth for
98 each species. Species are colored by class. **b** ASVs detected per patient for the most abundant species, also shown as a
99 function of sequencing depth. **c** Re-sampled data showing ASV distributions. **d** ASV diversity across different patients.
100 **e** ASV diversity across various time points.

101

102 **Supplementary File 1. List of microbe-metabolite/enzyme interactions predicted in early biofilms**

103 The rows represent relationships between taxa and other metabolites, enzymes or biofilm structures. For each
104 relationship, the object type, supporting evidence, comments, references, links to other databases and corresponding
105 visualization (either Fig. 7c or Supplementary Figure 5) are provided.

